



ELSEVIER

Physica D 137 (2000) 247–259

PHYSICA D

www.elsevier.com/locate/physd

Discrete singular convolution for the sine-Gordon equation

G.W. Wei*

Department of Computational Science, National University of Singapore, Singapore 119260, Singapore

Received 2 March 1999; received in revised form 29 July 1999; accepted 20 August 1999

Communicated by M. Sano

Abstract

This paper explores the utility of a discrete singular convolution (DSC) algorithm for the integration of the sine-Gordon equation. The initial values are chosen close to a homoclinic manifold for which previous methods have encountered significant numerical difficulties such as numerically induced spatial and temporal chaos. A number of new initial values are considered, including a case where the initial value is “exactly” on the homoclinic orbit. The present algorithm performs extremely well in terms of accuracy, efficiency, simplicity, stability and reliability. ©2000 Elsevier Science B.V. All rights reserved.

Keywords: Discrete singular convolution; Sine-Gordon equation; Homoclinic orbit

1. Introduction

Recent work by Ablowitz et al. [1,2] has pointed out the problem of numerically induced spatial and temporal chaos in numerical solutions of nonlinear wave equations such as the sine-Gordon equation [1], the nonlinear Schrödinger equation [3–5] and the modified Korteweg–de Vries (KdV) equation [6]. A serious implication is that at least some previous reports of chaos, in fact, are numerical artifacts. This problem might affect the mathematical modeling of many real problems in physics, chemistry, biology and engineering. Mathematically, for an integrable system, such numerical instability is associated with singularities in so-called phase space action–angle variables, which produce homoclinic orbits in the related phase space geometry [1–5,7–9]. The numerical solution near the

homoclinic orbits can be exponentially unstable [1] due to the frequent visiting of two solutions on “opposite sides” of the homoclinic orbit. This visiting or homoclinic orbit crossing can result from extremely small perturbations in the numerical parameters and/or from numerical errors in the calculated solution.

Conceptually, such “visiting” differs very much from the Gibbs’ oscillations occurring in spectral method approximations of a step function or in the numerical solution of Burgers’ equation with a high Reynolds number. The Gibbs’ oscillations are usually very regular but the homoclinic orbit crossing is, in general, very irregular. Moreover, the homoclinic orbit crossing is induced by the presence of phase space singularities, whereas Gibbs’ oscillations are caused by the sharp spatial changes in *real space* solutions over a small region such as a boundary layer. There, however, is a universal feature of these instabilities from the point of view of numerical integration. Essentially, instabilities typically occur when

* Tel.: +65-874-6589; fax: +65-774-6756.

E-mail address: cscweigw@nus.edu.sg (G.W. Wei).

the numerical algorithm with the given space and time meshes is not adequate for describing the actual solution. In many cases, the rate of convergence of a given method simply cannot match the rate of divergence of a solution near the singularity.

Recent analysis by Ablowitz et al. [2] found that pseudo-spectral methods perform significantly better for the Sine-Gordon equation than lattice type, symplectic schemes. From this result they concluded that numerical accuracy for approximating the spatial derivatives is more important than the symplectic schemes for the numerical integration of a general class of nonlinear wave equations. The importance of this result is obvious. However, computationally, for nonlinear equations, the global spectral and pseudo-spectral methods are not nearly as simple and robust to implement as various local methods. Moreover, global methods can only be directly used in structured grids. For unstructured grids, which are required for the case of complex geometry and boundary, only local methods can be directly implemented. Therefore, it would be extremely desirable to have accurate, efficient, and robust approaches for solving the various nonlinear wave equations which play an important role in modern science and technology. Wavelet theory has been expected to fulfill this task and has been extensively studied recently for this purpose [10–13], including the recently reported adaptive wavelet algorithms [14,15]. However, these efforts have been hindered either by the technical difficulties of incorporating multiresolution analysis into the treatment of boundary conditions or by the lack of accurate and efficient wavelets for solving linear and nonlinear partial differential equations (PDEs). For example, Beylkin and Keiser [14] reported the difficulty of handling the KdV equation by using a sophisticated wavelet algorithm.

Discrete singular convolution (DSC) [16] is a potential approach for numerically solving a few classes of problems, including Hilbert transform, processing of analytic signals, computational electromagnetics, computational tomography, and linear and nonlinear dynamics. In fact, underlying mathematical structure of DSC is the theory of distributions. One of the distributions used in the aforementioned applications is

the Dirac delta function which is a generalized function following from the fact that it is an integrable function inside a particular interval but it need not have a value. Heaviside introduced both the unit step Heaviside function and the Dirac delta function as its derivative, and referred to the latter as the unit impulse. Dirac, for the first time, explicitly discussed the properties of δ in his classic text on quantum mechanics; for this reason δ is often called Dirac delta function. However, delta distribution has a history which antedates both Heaviside and Dirac. It appeared in explicit form as early as 1822, in Fourier's *Théorie Analytique de la Chaleur*. The work of Heaviside, and subsequently of Dirac, in the systematic but informal exploitation of the step function and delta function has made delta distribution familiar to physicists and engineers before Sobolev, Schwartz [17], Korevaar [18,19] and others put it into a rigorous mathematical form. In particular, the Hermite function expansion of Dirac delta function was proposed by Schwartz [17] and Korevaar [20] over 40 years ago and was used by Hoffman et. al. [21] for numerical simulations. General orthogonal series analyses of the delta distribution have been subsequently studied by Walter [22] and others [23–25]. The use of many delta sequences as probability density estimators was discussed by Walter and Blum [25] and others [24,26,27].

The purpose of the present paper is to demonstrate that the discrete singular convolution (DSC) algorithm provides a powerful tool for solving the sine-Gordon equation. This paper is organized as follows. Section 2 is devoted to a brief review of the discrete singular convolution algorithm. Numerical integration of the sine-Gordon equation is given in Section 3. Particular attention is paid to those initial values which are close to the homoclinic orbits and have previously led to numerically induced spatial and temporal chaos. Concluding remarks are given in Section 4.

2. Discrete singular convolution

Singular convolutions appear in many science and engineering problems, such as Hilbert transform, Abel transform and Radon transform. Discrete singular

convolution is a unified approach for numerically solving singular convolution problems. The simplest way to introduce the theory of *singular convolution* (SC) is to work in the context of distributions. Let T be a distribution and $\eta(t)$ be an element of the space of test functions (e.g., $\eta(t) \in \mathcal{D}$). A singular convolution is defined as

$$F(t) = (T * \eta)(t) = \int_{-\infty}^{\infty} T(t-x)\eta(x) dx. \tag{1}$$

Here $T(t-x)$ is a singular kernel. Depending on the form of the kernel T , the singular convolution is the central issue for a wide range of science and engineering problems. For example, singular kernels of the *Hilbert type* have a general form

$$T(x) = \frac{1}{x^n} \quad (n > 0). \tag{2}$$

Here, kernels $T(x) = 1/x^a$ ($0 < a < 1$) define the *Abel transform* which is closely connected with a generalization of the tautochrone problem. Kernel $T(x) = 1/x$ is commonly encountered in electrodynamics, theory of linear response, signal processing, theory of analytic functions, and the Hilbert transform. Kernel $T(x) = 1/x^2$ is widely used in tomography. Other interesting examples are singular kernels of the *delta type*

$$T(x) = \delta^{(n)}(x) \quad (n = 0, 1, 2, \dots). \tag{3}$$

Here, kernel $T(x) = \delta(x)$ is important for the interpolation of surfaces and curves (including atomic, molecular and biological potential energy surfaces, aircraft and missile surfaces), and $T(x) = \delta^{(n)}(x)$ ($n = 1, 2, \dots$) are essential for obtaining weak solutions of partial differential equations. However, since these kernels are singular, they cannot be directly digitalized in computer. Hence, the singular convolution, (1), is of little numerical merit. To avoid the difficulty of using singular expressions directly in computer, sequences of approximations $\{T_\alpha\}$ of the distribution T can be constructed

$$\lim_{\alpha \rightarrow \alpha_0} T_\alpha(x) \rightarrow T(x), \tag{4}$$

where α_0 is a generalized limit. Obviously, in the case of $T(x) = \delta(x)$, the sequence, $T_\alpha(x)$, is a delta

sequence. Furthermore, with a sufficiently smooth approximation, it makes sense to consider a *discrete singular convolution* (DSC)

$$F_\alpha(t) = \sum_k T_\alpha(t-x_k)f(x_k), \tag{5}$$

where $F_\alpha(t)$ is an approximation to $F(t)$ and $\{x_k\}$ is an appropriate set of discrete points on which the DSC (5) is well defined. Note that the original test function $\eta(x)$ has been replaced by $f(x)$. The mathematical property or requirement of $f(x)$ is determined by the approximate kernel T_α . In general, the convolution is required being Lebesgue integrable.

A sequence of approximation can be improved by a regularizer [28,29]:

$$\lim_{\sigma \rightarrow \infty} R_\sigma(x) = 1. \tag{6}$$

The regularizer is designed to increase the regularity of convolution kernels. For the delta sequence, it follows from Eq. (4) that

$$\int \lim_{\alpha \rightarrow \alpha_0} T_\alpha(x)R_\sigma(x) dx = R_\sigma(0) = 1, \tag{7}$$

where $R_\sigma(0) = 1$ is the special requirement for a *delta regularizer*.

As an interesting example, Shannon’s kernel $\sin \alpha x / \pi x$ is a delta sequence kernel

$$\lim_{\alpha \rightarrow \infty} \left\langle \frac{\sin \alpha x}{\pi x}, \eta(x) \right\rangle = \eta(0). \tag{8}$$

Other important examples include the Dirichlet kernel

$$\frac{\sin [(l + \frac{1}{2})(x-x')]}{2\pi \sin [\frac{1}{2}(x-x')]},$$

the modified Dirichlet kernel

$$\frac{\sin [(l + \frac{1}{2})(x-x')]}{2\pi \tan [\frac{1}{2}(x-x')]},$$

and the de la Vallée Poussin kernel

$$\frac{1}{\pi \alpha} \frac{\cos [\alpha(x-x')] - \cos [2\alpha(x-x')]}{(x-x')^2}.$$

For sequences of both the delta type and the Hilbert type, an interpolating (or quasi interpolating) algorithm sampling at *Nyquist frequency*, $\alpha = \pi/\Delta$,

has a great advantage over a non-interpolating discretization

$$\frac{\sin [\alpha(x-x')] }{\pi(x-x')} \rightarrow \frac{\sin(\pi/\Delta)(x-x_k)}{(\pi/\Delta)(x-x_k)}. \tag{9}$$

The interpolating nature not only guarantees the highest accuracy on the set of grid points but also provides the highest possible computational efficiency of a grid. This is because the *Nyquist interval* given by $[-\pi/\Delta, \pi/\Delta]$ is the largest possible sampling interval that is free of alias whenever the L^2 function $f(x)$ under study satisfies the *Nyquist condition*:

$$\text{supp} \hat{f}(k) \subset \left\{ -\frac{\pi}{\Delta}, \frac{\pi}{\Delta} \right\}. \tag{10}$$

This fact can be formally given by Shannon’s sampling theorem

$$f(x) = \sum_{k=-\infty}^{\infty} f(x_k) \frac{\sin(\pi/\Delta)(x-x_k)}{(\pi/\Delta)(x-x_k)}. \tag{11}$$

The significance of Shannon’s sampling theorem is that by a discrete but infinite set of sampling data $\{f(x_k)\}$, one can actually recover a bandlimited L^2 function on the real line. Shannon’s sampling theorem has great impact on information theory, signal and image processing because the Fourier transform of Shannon’s kernel is an ideal low-pass filter for signals bandlimited to $[-\pi/\Delta, \pi/\Delta]$.

The uniform, Nyquist rate, interpolating discretization is also used for the Dirichlet kernel:

$$\frac{\sin [(l + \frac{1}{2})(x-x')] }{2\pi \sin [\frac{1}{2}(x-x')] } \rightarrow \frac{\sin((\pi/\Delta)(x-x_k))}{(2M+1) \sin((\pi/\Delta)((x-x_k)/(2M+1)))}. \tag{12}$$

In a comparison to Shannon’s kernel, the Dirichlet kernel has one more parameter M which can be optimized to achieve better results in computations. Usually, we set a sufficiently large M for various numerical applications. Obviously, the Dirichlet kernel converts to Shannon’s kernel at the limit $M \rightarrow \infty$. This uniform interpolating discretization will also be used for discretizing the modified Dirichlet kernels

$$\frac{\sin [(l + \frac{1}{2})(x-x')] }{2\pi \tan [\frac{1}{2}(x-x')] } \rightarrow \frac{\sin((\pi/\Delta)(x-x_k))}{(2M+1) \tan((\pi/\Delta)((x-x_k)/(2M+1)))}, \tag{13}$$

and for the de la Vallée Poussin kernels

$$\frac{1}{\pi\alpha} \frac{\cos [\alpha(x-x')] - \cos [2\alpha(x-x')]}{(x-x')^2} \rightarrow \frac{2}{3} \frac{\cos(\pi/\bar{\Delta})(x-x_k) - \cos(2\pi/\bar{\Delta})(x-x_k)}{[(\pi/\bar{\Delta})(x-x_k)]^2}, \tag{14}$$

where $\bar{\Delta} = \frac{3}{2}\Delta$. Since π/Δ is proportional to the highest frequency which can be reached in the Fourier representation, the Δ should be very small for a given problem involving very oscillatory functions or very high frequency components.

We use a symmetrically (or antisymmetrically) truncated, translationally invariant singular kernel

$$f^{(n)}(x) \approx \sum_{k=-W}^W \delta_{\alpha}^{(n)}(x-x_k) f(x_k) \quad (n = 0, 1, 2, \dots), \tag{15}$$

where $\{x_k\}$ are centered around x and $2W+1$ is the computational bandwidth, or effective kernel support, which is usually smaller than the whole computational domain $[a, b]$. Here $\delta_{\alpha}^{(n)}(x-x_k)$ is a collective symbol for the n th derivative of any of the right-hand side of Eqs. (9) and (12)–(14).

In the DSC approach, it is convenient to discretize an operator on a grid of the coordinate representation. This is illustrated by using a Hamiltonian. As such, the potential part, $V(x)$, of the Hamiltonian is diagonal. Hence, its discretization is simply given by a direct interpolation on the grid

$$V(x) \rightarrow V(x_k) \delta_{m,k}. \tag{16}$$

The differentiation matrix of an operator or the Hamiltonian on the coordinate grid is then given in terms of functional derivatives

$$-\frac{\hbar^2}{2\mu} \frac{d^2}{dx^2} \rightarrow -\frac{\hbar^2}{2\mu} \delta_{\alpha}^{(2)}(x_m - x_k), \tag{17}$$

where μ is the mass of the Hamiltonian system and $\delta_\alpha^{(2)}(x_m - x_k)$ are *analytically* given by

$$\delta_\alpha^{(2)}(x_m - x_k) = \left[\left(\frac{d}{dx} \right)^2 \delta_\alpha(x - x_k) \right]_{x=x_m}. \quad (18)$$

Thus, the full DSC grid representation for the Hamiltonian operator, H , is given by

$$H(x_m, x_k) = -\frac{\hbar^2}{2\mu} \delta_\alpha^{(2)}(x_m - x_k) + V(x_m) \delta_{m,k}. \quad (19)$$

All other operators which consist of a non-diagonal differentiation part and/or a diagonal part can be treated similarly.

In the present study we limit our attention to the singular kernels of Shannon (Shannon), the de la Vallée Poussin (DLVP), Dirichlet (Dirichlet) and the modified Dirichlet (MD). Nevertheless, various other delta sequence kernels can be similarly employed. It is noted that the singular kernels of Shannon (Shannon) and de la Vallée Poussin (DLVP) are parameter free, which is convenient for applications. The $2M + 1$ parameter used for the other two kernels is chosen as 71 for all calculations. We note that as long as the $2M + 1$ value is chosen sufficiently large ($2M + 1 > W$, where $2W + 1$ is the matrix bandwidth), the numerical results are not sensitive to the specific values used. The time discretization is obtained by using the fourth order Runge–Kutta scheme.

3. Application and results

The sine-Gordon equation is one of the most important nonlinear wave equations that can be used to model the soliton waves in nature. Although Stokes [30] described in detail the Stokes waves in 1847, the formal development of soliton theory was in 1960s [31–33]. Benjamin studied the instability of Stokes waves in deep water. Such an instability is also described by the nonlinear Schrödinger equation. Zabusky and Kruskal [32] pioneeringly studied the instability in the Korteweg–de Vries (KdV) equation describing nonlinear waves in shallow water [34,35]. A variety of other natural phenomena can be modeled

by the sine-Gordon equation. These include the rotator phase dynamics of the n -heneicosane ($C_{22}H_{44}$) polymer [36], H – D exchange in DNA [37,38] and r.f. radiation from a Josephson junction [39]. The numerical instability of nonlinear wave equations, including numerically induced spatial and temporal chaos of these equations, has been carefully investigated by Ablowitz et al. [1–4] recently. The purpose of this section is both to test the accuracy and reliability of the DSC algorithm for temporal integration of nonlinear wave equations and to numerically study the waveforms of the sine-Gordon equation when the initial values are either exponentially close to or “exactly” on the most unstable homoclinic orbit.

The sine-Gordon equation is given by

$$\frac{\partial^2 u(x, t)}{\partial t^2} - \frac{\partial^2 u(x, t)}{\partial x^2} + \sin[u(x, t)] = 0 \quad (20)$$

with periodic boundary conditions

$$u(x, t) = u(x + L, t). \quad (21)$$

It is a completely integrable Hamiltonian system [1,7] and the associated Hamiltonian can be defined as

$$H = \int_0^L \left[\frac{1}{2} v^2 + \frac{1}{2} \left(\frac{\partial u}{\partial x} \right)^2 + 1 - \cos(u) \right] dx. \quad (22)$$

The sine-Gordon Hamiltonian operator maps from the infinite dimensional phase space

$$F^{(L)} = \left\{ \mathbf{u}(x) = \begin{pmatrix} u(x) \\ v(x) \end{pmatrix}, e^{iu(x+L)} = e^{iu(x)}, \right. \\ \left. v(x + L) = v(x) \right\} \quad (23)$$

to the real line R . Here $v = u_t$ and u are related to the phase space variable (q, p) according to $q = u$ and $p = v$. It is noted that Hamilton’s equations hold as

$$\frac{\partial q}{\partial t} = \frac{\delta H}{\delta p}, \quad \frac{\partial p}{\partial t} = -\frac{\delta H}{\delta q}. \quad (24)$$

Ercolani et al. [7] analyzed the sine-Gordon phase space geometry. In particular, homoclinic orbits were shown to be associated with numerical instabilities [1,7] and even chaos. The simplest homoclinic orbit

can be obtained by examining the spatially homogeneous sine-Gordon equation, i.e., the periodic pendulum equation

$$\frac{\partial^2 u}{\partial t^2} + \sin(u) = 0. \quad (25)$$

The pendulum equation is integrable and has a well-known homoclinic orbit

$$u(x, t) = \pi - 4 \tan^{-1}[e^{(t+t_0)}] \quad (26)$$

corresponding to the phase space separatrix at $(\pi, 0)$. A family of homoclinic orbits can be constructed [1,6] by using the sine-Gordon symmetry

$$(x, t, u) \rightarrow (t, x, u + \pi). \quad (27)$$

By doing this one starts with a breather solution

$$u(x, t) = 4 \tan^{-1} \left[\frac{\tan(\nu) \cos[\cos(\nu)t]}{\cosh[\sin(\nu)x]} \right], \quad (28)$$

where the parameter ν satisfies

$$|\nu| \ll 1. \quad (29)$$

This breather can be viewed as a kink–antikink bounded pair in space with a $2\pi/\cos(\nu)$ periodic oscillation in time. The sine-Gordon space–time symmetry (27) leads to a family of real valued homoclinic orbits

$$u(x, t) = \pi + 4 \tan^{-1} \left[\frac{\tan(\nu) \cos[\cos(\nu)x]}{\cosh[\sin(\nu)t]} \right]. \quad (30)$$

In contrast to the spatially homogeneous homoclinic orbit, Eq. (26), this family of homoclinic orbits also has a $2\pi/\cos(\nu)$ periodic spatial structure, i.e., a tangent cone associated with the phase space limit point $(\pi, 0)$. We refer the reader to Ref. [7] for the construction of more general homoclinic states and a detailed spectral analysis.

For numerical purpose, the sine-Gordon equation (20) is rewritten as a pair of coupled equations

$$\begin{aligned} \frac{\partial u(x, t)}{\partial t} &= v(x, t), \\ \frac{\partial v(x, t)}{\partial t} &= \frac{\partial^2 u(x, t)}{\partial x^2} - \sin u(x, t). \end{aligned} \quad (31)$$

Two types of initial conditions are used in the present computations: one is chosen to be extremely close to or

even “exactly” on the homoclinic orbits and the other corresponds to a case where there is a breather–kink and antikink transition. Both cases were used previously by Ablowitz et al. [1] to demonstrate the possible appearance of numerical chaos. However, they did not provide stable numerical waveforms of the system.

3.1. Near homoclinic orbit states

We first consider the numerical solution of Eq. (20) with the initial values [1]

$$u(x, 0) = \pi + \epsilon \cos(\mu x), \quad u_t(x, 0) = 0, \quad (32)$$

with $\mu = 2\pi/L$ and $L = 2\sqrt{2}\pi$. It is noted that the value of π is numerically generated as $\cos^{-1}(-1)$ to the normal double precision. For this reason we use the quotation marks for the word *exactly* when we say exactly on the homoclinic orbit. The periodic boundary condition, Eq. (21), is numerically implemented. Ablowitz et al. [1] showed that for small ϵ 's, these initial values are exponentially close to the homoclinic manifold and produce numerical instability when one uses the Hirota algorithm [40], which is a doubly discrete, integrable discretization scheme standardly used in numerical integration of nonlinear wave equations. When ϵ was chosen to be small, both spatial and temporal chaos were easily excited by very small perturbations, even on the order of round-off error. These authors found a more troubling aspect that these numerical instabilities persisted as the mesh were refined and cannot be detected by monitoring the conserved quantities of the equation. In other words, the temporal evolution of the numerical solution remained unstable even if all the conserved quantities were well preserved (by employing a very fine grid). They showed that the chaos persists even if a spatially completely integrable scheme is employed.

To demonstrate the numerical stability of the DSC algorithm, we first consider those two ϵ values ($\epsilon = 0.05, 0.1$) that have previously been used by Ablowitz et al. [1]. In the case of $\epsilon = 0.05$, Ablowitz et al. [1] found numerically induced chaos in a very early time of the integration by using 64 grid points. As plotted in Fig. 1, the DSC algorithm produces stable wave forms even if a small number of grid points is chosen as

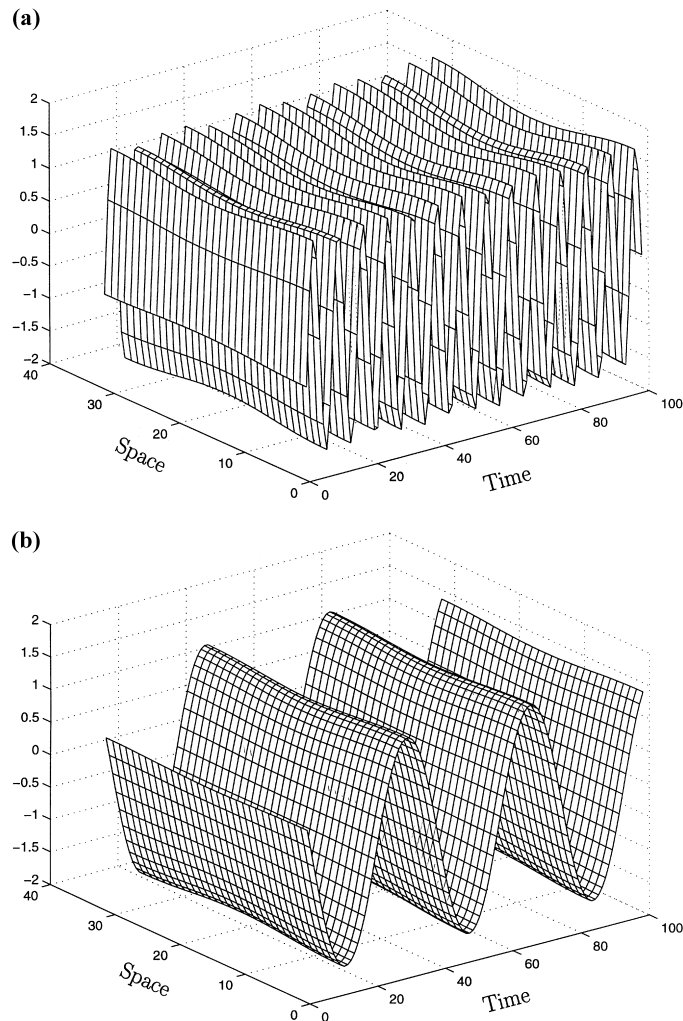


Fig. 1. The DSC solution of the sine-Gordon equation ($\epsilon = 0.05$, $N = 32$, $\tau = 0.02$): (a) between $t = 100$ and $t = 200$; (b) between $t = 10000$ and $t = 10020$.

$N = 32$. Obviously no irregular oscillation occurred in our results. Actually, no trace of any numerical instability has been detected even when the waveforms are integrated up to 10020 time units.

The case of $\epsilon = 0.1$ was also studied by Ablowitz et al. [1]. In particular, they found that this initial value led to numerically induced spatial and temporal chaos after a relatively longer time integration ($t \geq 300$ time units). In the present study, we still choose a relatively large grid mesh ($N = 32$) for the delta sequence kernels. As plotted in Fig. 2, there is no trace of numerical instability in our results. In fact, our DSC solution is

regular and stable even if the wave form is propagated to 10020 time units (see Fig. 2b).

To verify our results, we further consider a large ϵ value ($\epsilon = 1000$). This value is far from the low order homoclinic manifold. As expected, our results are still very stable even up to 10020 time units. These are depicted in Fig. 3. It is noted that when large ϵ values are used, the corresponding sine-Gordon waveforms are highly oscillative in the spatial domain.

For the last test, we choose $\epsilon = 0$ so that the initial values for the sine-Gordon equation is “exactly” on the most unstable homoclinic manifold. Surprisingly, we

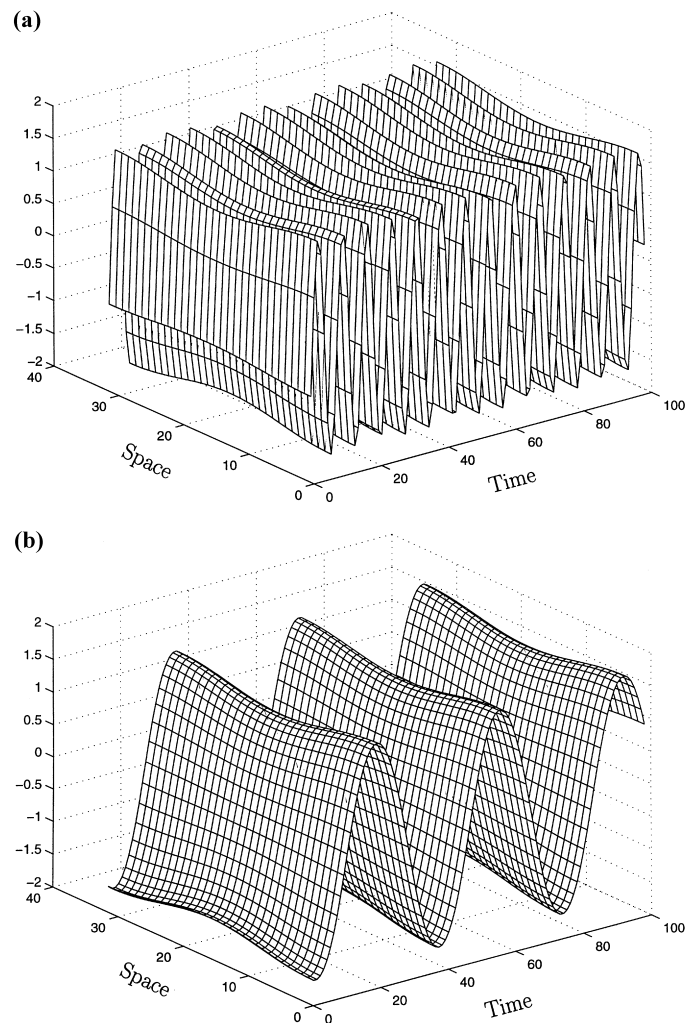


Fig. 2. The DSC solution of the sine-Gordon equation ($\epsilon = 0.1$, $N = 32$, $\tau = 0.02$): (a) between $t = 100$ and $t = 200$; (b) between $t = 10000$ and $t = 10020$.

obtain another set of stable waveforms for this initial value as given in Fig. 4, which is free from any trace of numerical instability.

By a comparison of waveforms for various ϵ values from 0 to 1000, we conclude that all of the results are consistent with each other and sound. All results in these figures are obtained by using 32 grid points and a time mesh of $\tau = 0.02$. Note that we have fixed the number of plots as 100 in all figures. To confirm our results further, we have also tested a number of different initial values ($\epsilon = 0.001$, 1, and 100), a number of different (even and odd) grid points and some

very small or large time meshes, such as $\tau = 0.00001$, 0.25. We have also changed the number of plots and integration time units. All of these results are stable, and consistent with regard to these variations.

Our results are completely regular and free of numerical instability for all four delta sequence kernels numerically tested in this work. We noted that graphically, there was no difference between the results obtained by employing any of the delta sequence kernels of Shannon, Dirichlet and modified Dirichlet. We have also obtained the same type of results by means of the de la Vallée Poussin delta sequence kernel using

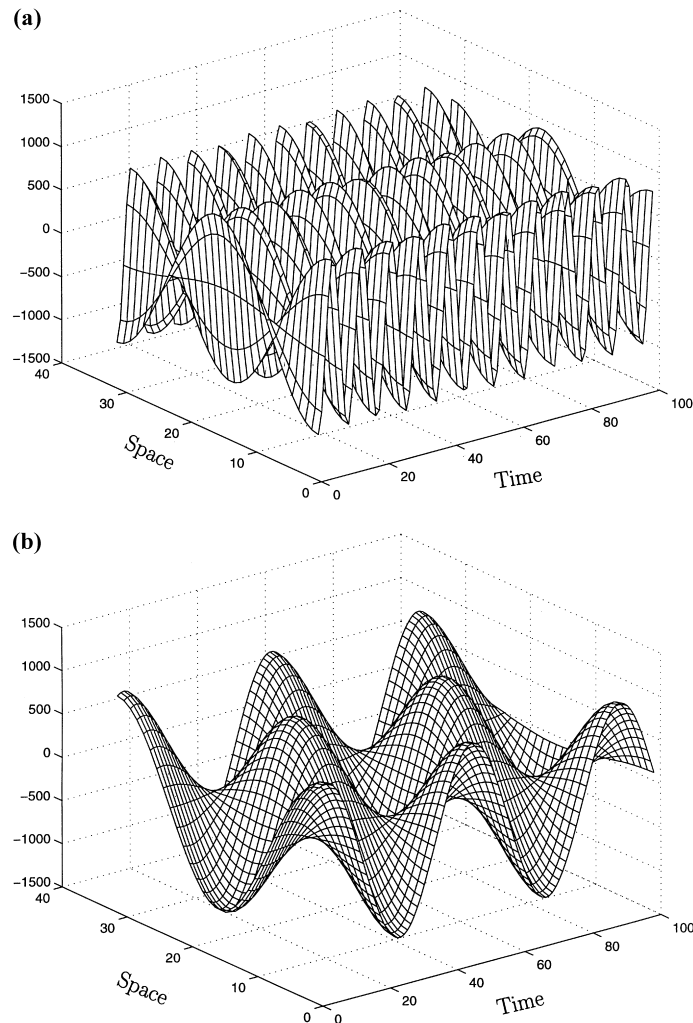


Fig. 3. The DSC solution of the sine-Gordon equation ($\epsilon = 1000.0$, $N = 32$, $\tau = 0.02$): (a) between $t = 100$ and $t = 200$; (b) between $t = 10000$ and $t = 10020$.

slightly more grid points. These results provide very strong evidence that the DSC algorithm is very reliable and robust for integrating nonlinear wave equations with low-lying unstable homoclinic orbits. As is well known, the low-lying homoclinic orbits are most easily excited by extremely small perturbations, even the computer round-off errors for the sine-Gordon equation. Ablowitz et al. [1] pointed out that occurrence of numerical chaos is primarily the result of inaccurate approximation of the spatial derivatives in discretizing the partial differential equation [2]. Hence, the present DSC algorithm must provide very high accuracy for

approximating the spatial derivatives. This is consistent with our results on eigenvalue problems of the Schrödinger equation and the Fokker–Planck equation where the second order derivative is required.

3.2. Breather-kink and antikink transition

To explore the accuracy and reliability of the DSC algorithm for the integration of the sine-Gordon equation further, we consider different initial values where previous work indicates the occurrence of a different type of numerical instability [1]. The analytical

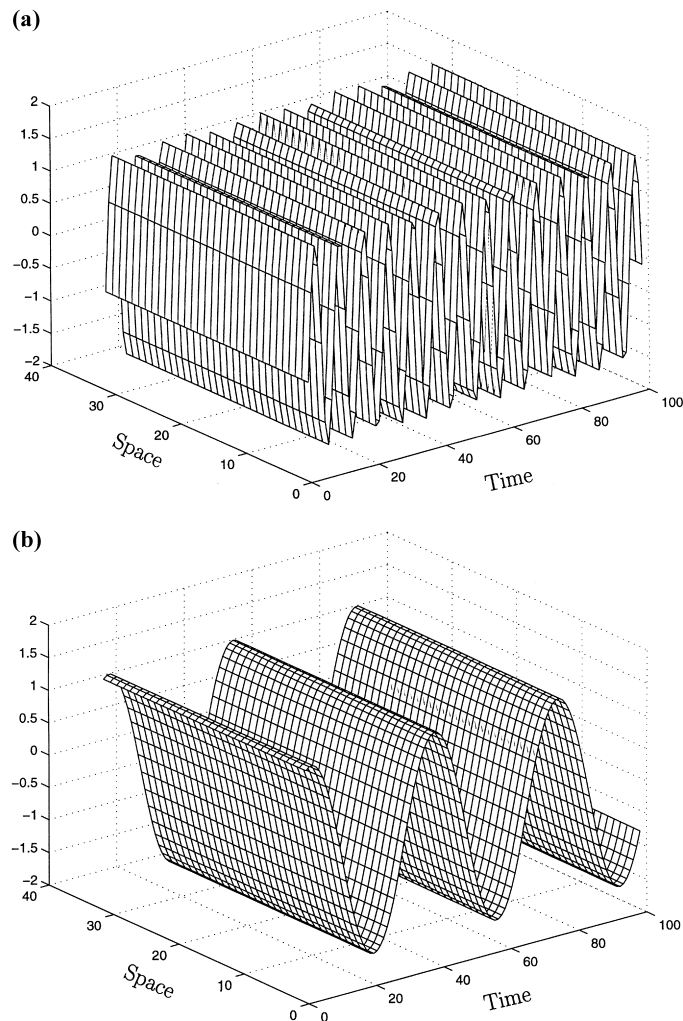


Fig. 4. The DSC solution of the sine-Gordon equation ($\varepsilon = 0.0$, $N = 32$, $\tau = 0.02$): (a) between $t = 100$ and $t = 200$; (b) between $t = 10000$ and $t = 10020$.

solution represents a breather-kink and antikink transition associated with a double point in the nonlinear spectrum of the sine-Gordon equation [1]:

$$u(x, t) = 4 \tan^{-1} [\operatorname{sech}(x)t], \quad -\infty < x < \infty, \quad (33)$$

with initial values

$$u(x, 0) = 0, \quad u_t(x, 0) = 4 \operatorname{sech}(x), \quad (34)$$

and periodic boundary conditions. In this case the solution is far away from the unstable homoclinic manifolds. Using the doubly discrete, integrable discretization scheme [40], Ablowitz et al. [1] found that

numerically induced chaos occurred for 64 grid points after a number of integrations. However, unlike the previous examples of their calculations, the chaos disappeared when a refined grid mesh ($N = 128$) was employed. A careful examination of their results indicates that the breather-kink and antikink transition occurred much earlier than it should in their refined calculation. This phenomena can be characterized as *numerical catalyzed breather-kink and antikink transition*. In our calculation, a total of 64 grid points ($N = 64$) is used in the interval $[-20, 20]$ for the delta sequence kernels of Shannon, Dirichlet and modified

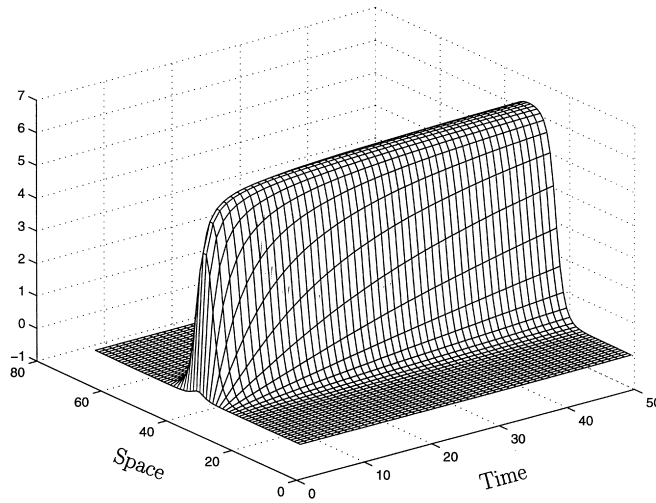


Fig. 5. Numerical and exact solution of the sine-Gordon equation with initial values (34) describing a breather-kink and antikink transition (between $t = 0.05$ and $t = 100$, $N = 64$, $\tau = 0.05$).

Dirichlet. To achieve the same level of accuracy, as many as 1.5 times of grid points ($N = 96$) are used for the de la Vallée Poussin delta sequence kernel. Both the exact results and the Dirichlet delta sequence kernel calculations obtained by using 64 grid points are plotted in Fig. 5. There is no visible difference in the two solutions. The computational results obtained by using other delta sequence kernels are graphically the same as that in Fig. 5. Actually, the present method provides smooth, stable numerical solutions by using 40 or even fewer grid points. The accuracy of the DSC algorithm for the sine-Gordon equation is controllable and the L_∞ and L_2 errors are very small with the present choice of spatial and temporal mesh sizes. These results are listed in Table 1. It is seen that the DSC algorithm achieves an accuracy of four or five

significant figures for the sine-Gordon equation using a reasonably small number of grid points and relatively large time increment.

4. Conclusion

By focusing on the delta sequence kernels of Shannon, Dirichlet, modified Dirichlet and the de la Vallée Poussin, the utility of the DSC algorithm is explored for the nonlinear dynamics of the sine-Gordon equation, which is a challenging case when the initial values are close to the homoclinic orbits. The DSC algorithm is used for spatial discretization which is in association with the fourth order Runge–Kutta scheme for time integration. We have chosen the

Table 1
 L_∞ and L_2 errors of the numerical solutions for the sine-Gordon equation

t	Shannon		Dirichlet		MD		DLVP	
	L_2	L_∞	L_2	L_∞	L_2	L_∞	L_2	L_∞
1.0	1.55(-4)	8.87(-5)	1.55(-4)	8.87(-5)	1.55(-4)	8.87(-5)	1.71(-4)	1.01(-4)
2.0	1.04(-3)	5.61(-4)	1.03(-3)	5.61(-4)	1.03(-3)	5.61(-4)	1.19(-4)	5.51(-5)
4.0	1.21(-3)	6.11(-4)	1.20(-3)	6.11(-4)	1.21(-3)	6.11(-4)	1.00(-4)	4.20(-5)
6.0	9.05(-4)	4.02(-4)	9.05(-4)	4.02(-4)	9.05(-4)	4.02(-4)	1.25(-4)	4.40(-5)
8.0	1.35(-3)	6.37(-4)	1.35(-3)	6.37(-4)	1.35(-3)	6.37(-4)	1.14(-4)	3.82(-5)
10.0	1.88(-3)	7.63(-4)	1.88(-3)	7.63(-4)	1.88(-3)	7.63(-4)	1.32(-4)	4.91(-5)

sine-Gordon equation because Ablowitz et al. [2] have recently called attention to the numerical difficulties of this problem. They showed that when initial values are chosen to be close to the homoclinic manifolds, previous integrable discretization schemes encountered difficulties, including numerically induced spatiotemporal chaos [1]. There is no report on the numerical method which is totally free from homoclinic-orbit-crossing in the literature.

A number of new initial values are considered, including a case where the initial value is “exactly” on the homoclinic orbit. Important numerical issues examined in this paper are the accuracy of approximation, the speed of convergence, the simplicity of implementation, the stability of integration and the reliability of application. The DSC algorithm performs extremely well for all issues.

For two troubling initial values which are close to the sine-Gordon homoclinic orbit and have been used previously by Ablowitz et al. [2], the DSC algorithm provides stable, smooth, chaos free and even homoclinic-orbit-crossing free results by using a small number of grid points ($N = 32$). In both cases we actually integrate the waveforms up to 10020 time units without encountering any trace of numerical instability. To verify our results, we consider ϵ values as large as 1000. There is still no trace of numerical instability in our solution for this case. In a dramatic case, the initial value is chosen to be “exactly” on the homoclinic orbit ($\epsilon = 0$). Our DSC results remain smooth, stable, and consistent with those obtained with non-zero ϵ values. Our results are verified by using a variety of different time meshes, number of grid points, number of plots and integrating time units. The complete dynamical behavior of the sine-Gordon equation with this set of initial values can be understood from our numerical simulations.

The other type of initial values considered in this work is the situation where a solitary transition from a breather to a kink and antikink occurs during the time evolution of the sine-Gordon soliton. Numerically induced spatial chaos was also reported in the literature for this problem [1] when the number of grid points is chosen as $N = 64$ in the interval of $[-20, 20]$. The DSC algorithm provides stable results by using only

40 grid points in the same interval. Our DSC results are accurate up to five significant figures for this initial value using a slightly larger number of grid point ($N = 64$) in the interval of $[-20, 20]$ and a relatively large time increment of 0.05.

Since the symplectic numerical schemes are designed to preserve the phase space structures of Hamiltonian systems, they have been the main focus of enormous research in the past and have been regarded as superior to explicit methods such as the Runge–Kutta scheme. Only very recently after a systematical comparison of a number of numerical schemes have Ablowitz et al. [2] pointed out that the accuracy of the spatial discretization is more important than the symplectic property. The superior results obtained in this work indicate that the DSC algorithm provides highly accurate spatial discretizations for integrating nonlinear partial differential equations. However, it is our experience that not only the accuracy but also the implementation of a numerical algorithm that determine the numerical stability for integration of nonlinear wave equations. This point will be formally explored in our future work.

Acknowledgements

This work is supported in part by the National University of Singapore. The correspondence with Prof. M.J. Ablowitz and discussion with Prof. C. Schober about the sine-Gordon equation are gratefully acknowledged.

References

- [1] M.J. Ablowitz, B.M. Herbst, C. Schober, *J. Comput. Phys.* 126 (1996) 299.
- [2] M.J. Ablowitz, B.M. Herbst, C. Schober, *J. Comput. Phys.* 131 (1997) 354.
- [3] B.M. Herbst, M.J. Ablowitz, *Phys. Rev. Lett.* 62 (1989) 2065.
- [4] M.J. Ablowitz, B.M. Herbst, *SIAM J. Appl. Math.* 50 (1990) 339.
- [5] D.W. McLaughlin, C.M. Schober, *Physica D* 57 (1992) 447.
- [6] B. Fornberg, G.B. Whitham, *Phil. Trans. R. Soc. London A* 289 (1978) 373.
- [7] N. Ercolani, M.G. Forest, D.W. McLaughlin, *Physica D* 43 (1990) 349.

- [8] A.R. Bishop, M.G. Forest, D.W. McLaughlin, E.A. Overman II, *Physica D* 23 (1986) 293.
- [9] M.G. Forest, C.G. Goedde, A. Sinha, *Physica D* 67 (1993) 347.
- [10] R.L. Schult, H.W. Wyld, *Phys. Rev. A* 46 (1992) 12.
- [11] J. Liandrat, V. Perrier, P. Tchamitchian, in: M.B. Ruskai, G. Beylkin, R. Coifman, I. Daubechies, S. Mallat, Y. Meyer, L. Raphael (Eds.), *Wavelets and their Applications*, Jones & Bartlett, Boston, 1992.
- [12] B. Jawerth, W. Sweldens, *SIAM Rev.* 36 (1994) 377.
- [13] W.K. Liu, *Int. J. Numer. Meth. Fluids* 21 (1995) 901.
- [14] G. Beylkin, J. Keiser, *J. Comput. Phys.* 132 (1997) 233.
- [15] J. Fröhlich, K. Schneider, *J. Comput. Phys.* 130 (1997) 174.
- [16] G.W. Wei, *J. Chem. Phys.* 110 (1999) 8930.
- [17] L. Schwartz, *Théorie des Distributions*, Hermann, Paris, 1951.
- [18] J. Korevaar, *Nederl. Akad. Westensh. Proc. Ser. A* 8 (1955) 368, 483, 663.
- [19] J. Korevaar, *Mathematical Methods*, vol. 1, Academic Press, New York, 1968.
- [20] J. Korevaar, *Am. Math. Soc. Trans.* 91 (1959) 53.
- [21] D.K. Hoffman, N. Nayar, O.A. Sharafeddin, D.J. Kouri, *J. Phys. Chem.* 95 (1991) 8299.
- [22] G.G. Walter, *Trans. Am. Math. Soc.* 116 (1965) 492.
- [23] G.W. Walson, M.R. Leadbetter, *Sankhya* 26 (1965) 101.
- [24] B.B. Winter, *Ann. Statist.* 3 (1975) 759.
- [25] G.G. Walter, J. Blum, *Ann. Statist.* 7 (1977) 328.
- [26] G. Wahba, *Ann. Statist.* 3 (1975) 15.
- [27] R. Kronmal, M. Tarter, *J. Am. Statist. Assoc.* 63 (1968) 925.
- [28] G.W. Wei, D.S. Zhang, D.J. Kouri, D.K. Hoffman, *Phys. Rev. Lett.* 79 (1997) 775.
- [29] G.W. Wei, *Chem. Phys. Lett.* 296 (1998) 215.
- [30] C.M. Stokes, *Cambridge Trans.* 8 (1847) 441.
- [31] T.B. Benjamin, *Proc. R. Soc. A* 299 (1967) 59.
- [32] N.J. Zabusky, M.D. Kruskal, *Phys. Rev. Lett.* 15 (1965) 240.
- [33] G.B. Whitham, *Linear and Nonlinear Waves*, Wiley, New York, 1974.
- [34] D.J. Korteweg, de Vries, *Phil. Mag.* 39 (1895) 422.
- [35] A.C. Newell, *Solitons in Mathematics and Physics*, SIAM, Philadelphia, PA, 1985.
- [36] D.C. Doherty, A.J. Hopfinger, *Phys. Rev. Lett.* 72 (1994) 661.
- [37] S. Yomosa, *J. Phys. Soc. Jpn.* 64 (1995) 1917.
- [38] W. Hai, *Phys. Lett. A* 186 (1994) 309.
- [39] O.H. Olsen, *Phys. Rev. E* 50 (1994) 182.
- [40] R. Hirota, *J. Phys. Soc. Jpn.* 43 (1977) 2079.